

Sol–gel synthesis of $\text{Mn}_2\text{O}_3/\text{Al}_2\text{O}_3/\text{SiO}_2$ hybrid nanocomposite and application for removal of organic dye

Mahboube Mohaghegh Motlagh · S. A. Hassanzadeh-Tabrizi · Ali Saffar-Teluri

Received: 22 May 2014 / Accepted: 27 August 2014 / Published online: 3 September 2014
© Springer Science+Business Media New York 2014

Abstract Nanocomposite of $\text{Mn}_2\text{O}_3/\text{Al}_2\text{O}_3/\text{SiO}_2$ was prepared through an in situ sol–gel process, in which Mn_2O_3 nanocrystals were dispersed in the silica-alumina amorphous matrix. The synthesized products were studied by X-ray diffraction, thermogravimetric and differential thermal analysis, Brunauer–Emmett–Teller surface area analysis, UV–Vis spectroscopy and transmission electron microscopy. The nanocomposite was applied as a novel adsorbent for removal of methylene blue dye and the effect of heat treatment and contact time were studied. The results showed that nano- Mn_2O_3 particles were distributed on the surface of $\text{Al}_2\text{O}_3/\text{SiO}_2$ and formed an activated surface charge. In addition, it was found that the nanocomposites removal rate strongly depended on the heat-treatment of adsorbent.

Keywords Nanocomposites · Sol–gel synthesis · Dye removal · Transmission electron microscopy

1 Introduction

The contamination of water has been a serious problem for governments and environmental scientists in last decades [1].

The waste water of the textile industries is known to contain a considerable large amount of azo dyes and inorganic salts. Among these pollutions, azo dyes are used for colorization in textile industries. Therefore, azo dyes removal in wastewater has attracted considerable attention because of their environmental toxicity and public health damage, which can lead to sensitivity, allergy and even intestinal cancer [2–4]. Different methods such as adsorption, photocatalysis, oxidation, electrolysis, etc. have been used to remove organic pollutants from wastewater [5, 6]. Among these various techniques for dye removal from wastewater, adsorption is an effective and economical method in low-concentration pollution treatment and operational convenience [7]. It is known that the removal capacity of an adsorbent mainly depends on its surface properties, including surface area and surface ion exchange sites [8]. Various adsorbents, such as nanoporous silica [9], hydroxyapatite/chitosan [10], Graphite oxide/chitosan [11], $\text{ZnO}-\text{Al}_2\text{O}_3$ [12] nano- MoS_2 /bentonite [13] and so on, have been investigated.

SiO_2 , Al_2O_3 and $\text{SiO}_2-\text{Al}_2\text{O}_3$ composite are widely used as catalyst supports and ceramic materials because of low thermal expansion and conductivity, low dielectric constant, etc. [14–16]. Transition metal oxides were used into these supports to improve their catalytic activities. Among the metal oxides, manganese oxide is one of the most attractive inorganic materials because of its excellent physical and chemical properties and wide applications in catalysis, ion exchange, molecular adsorption and biosensors [17]. For instance, $\text{Mn}_2\text{O}_3-\text{SiO}_2$ composite has been extensively used for many applications in terms of catalysts and adsorption [18, 19].

Numerous techniques such as, heterogeneous precipitation [12], co-precipitation [20], sol–gel [21], solvothermal [22] etc. have been proposed to synthesize these adsorbents. Sol–gel technology has been developed for the

M. M. Motlagh
Department of Materials Engineering, Najafabad Branch,
Islamic Azad University, Najafabad, Isfahan, Iran

S. A. Hassanzadeh-Tabrizi (✉)
Young Researchers and Elite Club, Najafabad Branch,
Islamic Azad University, Najafabad, Isfahan, Iran
e-mail: tabrizi1980@gmail.com; hassanzadeh@pmt.iaun.ac.ir

A. Saffar-Teluri
Department of Chemistry, Faculty of Science, Najafabad
Branch, Islamic Azad University, Najafabad, Isfahan, Iran

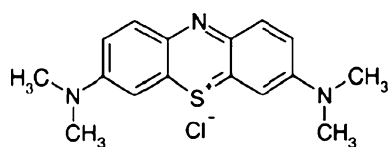


Fig. 1 Chemical structure of methylene blue

fabrication of high-quality nanocomposite powders. For complex powders, it achieves ultra-homogeneous of the several components on a molecular scale [23, 24].

In the present study, a new kind of adsorbent $\text{Mn}_2\text{O}_3/\text{Al}_2\text{O}_3/\text{SiO}_2$ was prepared by a sol–gel method. In fact, we employed $\text{Al}_2\text{O}_3/\text{SiO}_2$ hybrid as the composite support of Mn_2O_3 . Methylene blue (MB) serves as a model compound for common water-soluble azo dyes (Fig. 1), which are widely used in textile and chemical industries.

2 Experimental procedure

2.1 Materials and method

Manganese nitrate ($\text{Mn}(\text{NO}_3)_2 \cdot 4\text{H}_2\text{O}$) aluminum nitrate ($\text{Al}(\text{NO}_3)_3 \cdot 9\text{H}_2\text{O}$) and Tetraethylorthosilicate (TEOS) were used as manganese, aluminum and silicon precursors, respectively. All chemicals were purchased from Merck and used without further purification. 60 %wt Mn_2O_3 –20 %wt SiO_2 –20 %wt Al_2O_3 nanocomposite were prepared by sol–gel method. Molar ratio of TEOS, water, ethanol and HCl was 1:12:22:0.00079. The composite was prepared as follow: TEOS was firstly mixed with distilled water, ethanol and HCl; then manganese nitrate and aluminum nitrate were dissolved into the solution with stirring and heating. The solution became homogeneous, and the solution was stirred for 4 h. After aging for 24 h, the transparent gel was dried at 110 °C to remove water and any solvent, and then it was calcined different temperatures. The flow chart of the composite preparation is shown in Fig. 2.

2.2 Characterization

Differential thermal analysis (DTA) and thermogravimetry (TG) were used in the range of 25–950 °C with a rate of 10 °C/min with STA equipment (STA 1640). X-ray diffraction (XRD) measurements of the prepared samples were performed using a Philips X'pert model with $\text{CuK}\alpha$ radiation. The crystallite size (d) of the powder was measured from the Scherrer equation. The BET specific surface area of the samples was determined by N_2 adsorption–desorption on

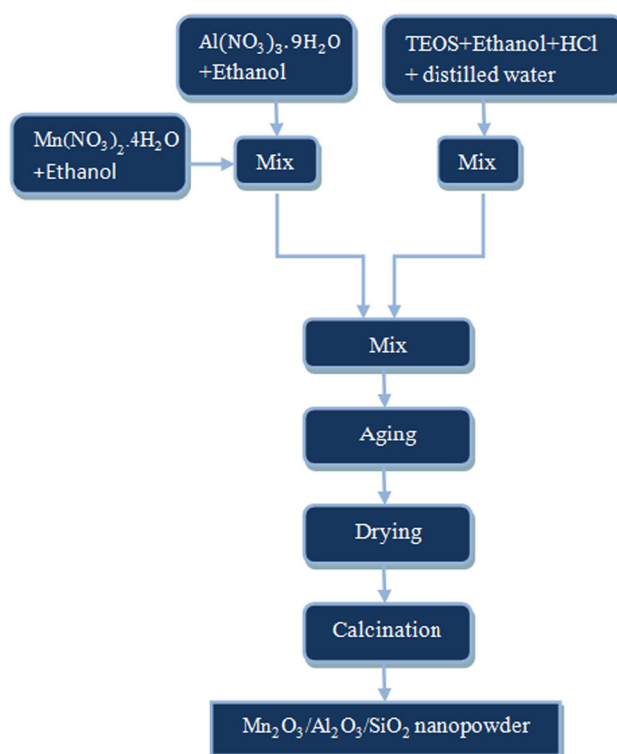


Fig. 2 Schematic diagram of the preparation of $\text{Mn}_2\text{O}_3/\text{Al}_2\text{O}_3/\text{SiO}_2$ nanopowder

a NOVA-2000 automated gas sorption system. TEM electron micrograph of the powders was recorded with a JEM-100CX transmission electron microscope.

2.3 Adsorption measurements

The removal experiments were carried out in an aqueous solution at room temperature. Adsorption of MB on nanocomposites calcined at different temperatures (500, 650, 850 °C) was studied. 0.001 g adsorbent was added to a glass flask containing 10 ml aqueous solution of MB (10 mg/l). The mixture was stirred magnetically at room temperature. At predetermined time intervals, the mixture was centrifuged in order to separate the dye solution from the adsorbent, and then the residual concentration of MB was measured with a UV–Vis spectrophotometer (UV–Vis spectrophotometer, Optizen 3220) at the wavelength of 664 nm. All experiments were carried three times. The removal rates (R) of MB were calculated from the following equation:

$$R = \frac{C_0 - C_t}{C_0} \times 100 \quad (1)$$

where C_0 is the initial concentration of MB, C_t is the instant concentration of MB at a predetermined time t .

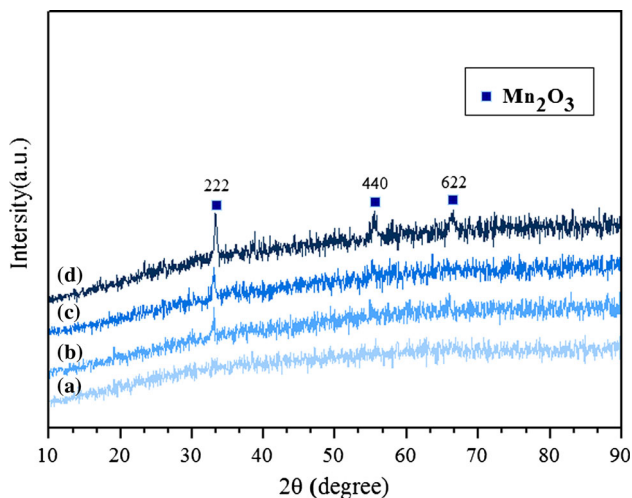


Fig. 3 XRD patterns of nanocomposites heat treated at different temperatures. *a* 110 °C, *b* 500 °C, *c* 650 °C and *d* 850 °C

3 Results and discussion

Figure 3 shows the XRD patterns recorded for the dried gel and the powders heat treated at 500, 650 and 850 °C. As can be seen, the gel dried at 110 °C seems to be amorphous. By increasing the heat treatment temperature, Mn₂O₃ with cubic structure is detected (JCPDS No. 89-4836). The peak intensity of Mn₂O₃ increases with increasing the temperature. In addition, the broadening of the peaks decreases, which shows growing the nanocrystallites. No diffraction peaks for Al₂O₃ were observed in the composite which shows it remains amorphous up to 850 °C. Some researchers reported that [25, 26], transition phases of Al₂O₃ in pure alumina is formed during heat treatment between 600 and 800 °C. The formation of crystallized transition alumina from amorphous alumina involves the rearrangement of the lattice to a cubic array. It was reported that impurities and second phases can be partially dissolved in alumina lattice because of the amorphous structure with a considerable number of defects and disorder [27]. It may exert dragging force on the diffusion of aluminum ions and hence the crystallization to transition phases of Al₂O₃ occurs at higher temperatures.

XRD crystallite size of the samples (d) can be estimated from XRD patterns by substituting the value of the full-width at half maximum (FWHM) of broadened characteristic peaks to Scherrer’s equation as follows:

$$d = \frac{0.9\lambda}{FWHM \cos(\theta)} \quad (2)$$

where λ is the X-ray wavelength and θ is the diffraction angle for the plane. The average crystallite size of samples

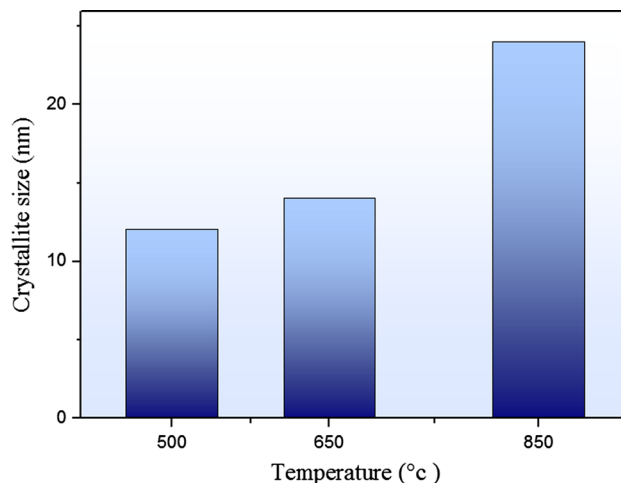


Fig. 4 Effect of calcination temperature on crystallite size

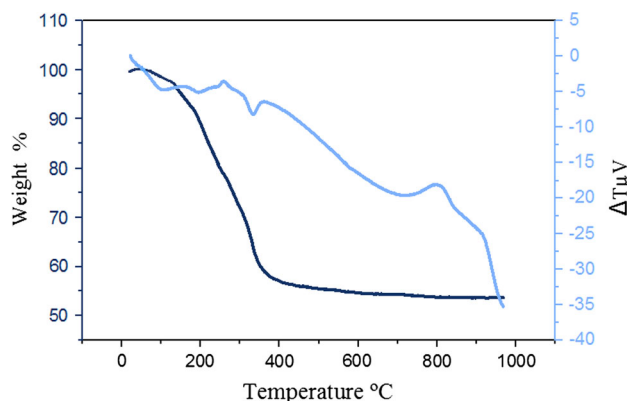


Fig. 5 DTA and TG curves of the samples

with different temperature is shown in Fig. 4. As can be seen, the crystallite size increases with increasing the calcination temperature. In addition, the growth rate of crystallites increases at higher temperatures.

Figure 5 shows the thermogravimetry and differential thermal analysis (TG–DTA) curves of the dried gels in air atmosphere. It can be seen that there are two weight loss stages in the TGA curve. In the first stage, mass loss of about, 5 % between 100 and 160 °C was observed which may be due to desorption of physisorbed water. The second weight loss step (40 %) is from 160 to 380 °C, arising from the evaporation and removal of water, ethanol and dehydration of the gel [28, 29]. In the DTA curve, two low intensity endothermic peaks at 120 and 180 °C were observed, which are attributed to the loss of adsorbed water and dehydration of the gel. Two exothermic peaks at 295 and 760 °C are attributed to the decomposition of residual organic solvents and crystallization,

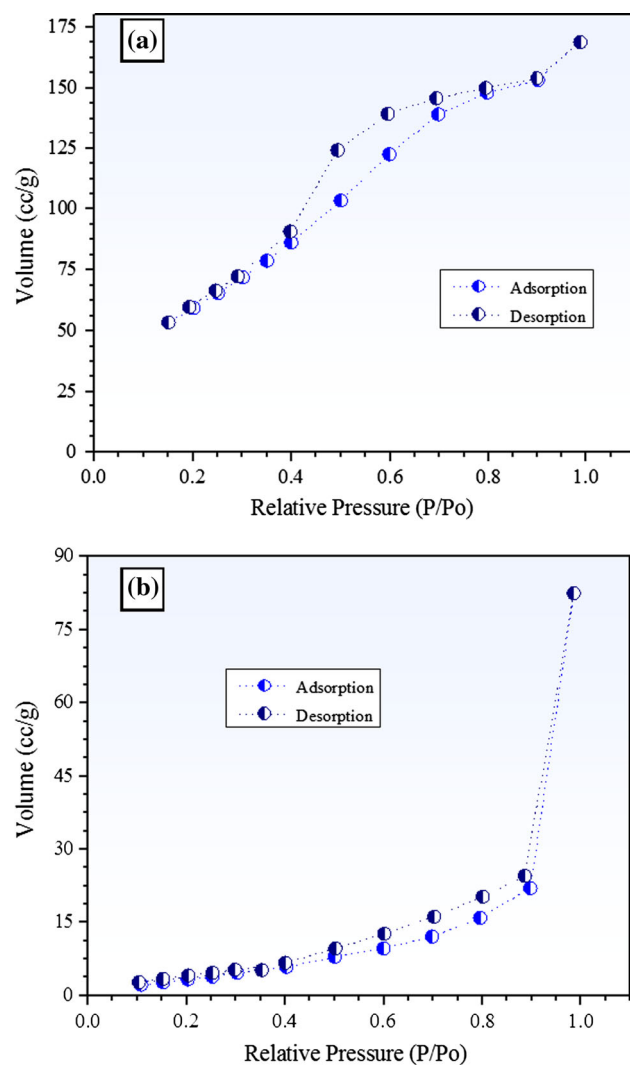


Fig. 6 Nitrogen adsorption–desorption isotherms upper insets of nanocomposites calcined at **a** 650 and **b** 850 °C

respectively [28, 30, 31]. The weight loss ends at about 500 °C so it can be chosen as the lowest calcination temperature in which the removal of organic materials is completed.

Figure 6 shows the N₂ adsorption–desorption isotherms of the composites calcined at 650 and 850 °C. The samples exhibit typical type IV isotherm according to the IUPAC classification, typical for mesoporous materials [32]. The existence of the hysteresis loop in the isotherms is due to the capillary condensation of N₂ gas occurring in the mesoporous. The textural properties of the samples obtained from the curves in Fig. 6 shows that the surface area of the powder calcined at 650 °C is 300 m²/g. The surface area of the powder decreases to 32.9 m²/g, by increasing the calcination temperature up to 850 °C, which could be related to sintering of particles.

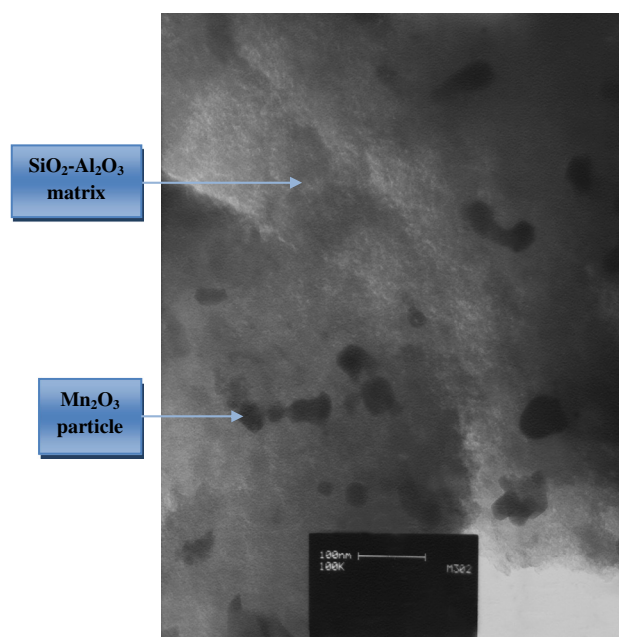


Fig. 7 TEM image of the sample calcined at 650 °C

TEM image of the sample calcined at 650 °C is shown in Fig. 7. As can be seen, Mn₂O₃ nanoparticles embedded in the amorphous silica-alumina matrix. This result is expected for silica composite materials modified with transition metals prepared via sol–gel method. For instance, Santos et al. [33] prepared silica–cobalt composites through sol–gel method and showed that there were segregated Co₃O₄ particles on the external surface of silica. The size of the majority of Mn₂O₃ nanoparticles in this nanocomposite varied between 18 and 61 nm. The Mn₂O₃ nanoparticles are almost spherical in shape. The calculated average size by Scherrer's equation was about 15 nm (Fig. 4). The discrepancy in the sizes from TEM and XRD results may be due to the fact that the Scherrer equation underestimates the crystallite size as it ignores the broadening of the diffraction peaks due to the microstrain in the lattice [34, 35].

Figure 8 shows the effect of heat treatment and contact time on adsorption of MB by nanocomposite samples. It is observed that there is an intense increase in the adsorption capacity of MB as the calcination temperature of nanocomposite increases from 500 to 650 °C, thereby indicating heat treatment temperature of composites had an important effect on the adsorption process. This may be due to the crystallinity of the composites which is low at 500 °C as shown in Fig. 3. It is also observed that adsorption capacity of MB decreased with the increasing of heat treatment temperature up to 850 °C, which may be attributed to the decrease in the surface area of the samples and grain

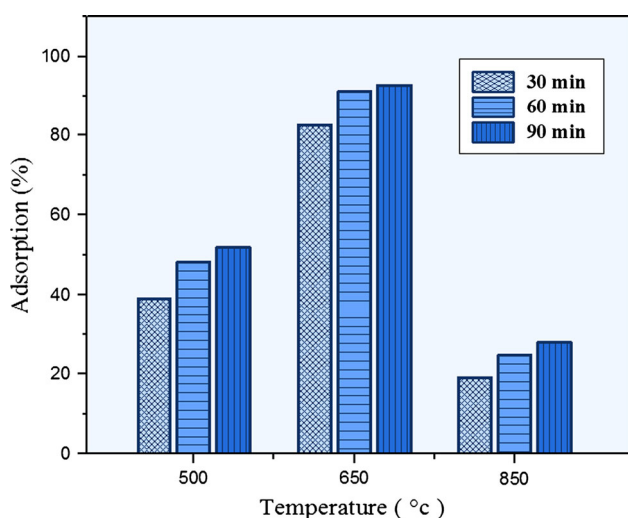


Fig. 8 Effect of heat treatment and contact time on adsorption of MB

growth. In addition, equilibrium time is one of the most important parameters in the design of economical wastewater treatment systems. It can be seen in Fig. 8 that adsorption capacity increased with increasing contact time. Large amounts of MB were removed in the first 30 min and equilibrium was reached in 90 min. After the equilibrium, adsorption efficiency was not increased significantly. The rapid adsorption at the initial contact time may be due to the abundant availability of active sites on the composite surface. With the increase of contact time, these sites are gradually occupied, therefore, the adsorption becomes less efficient [36].

4 Conclusion

$\text{Mn}_2\text{O}_3/\text{Al}_2\text{O}_3/\text{SiO}_2$ nanocomposite was prepared via an in situ sol–gel process. The new adsorbent shows excellent adsorption capacity for methylene blue dye. The resulting composite was characterized by different analytical techniques such as DTA–TG, BET, TEM, UV–Vis and XRD. The adsorption of methylene blue as a function of contact time and calcination temperature of the composites was investigated. The results showed Mn_2O_3 nanoparticles of about 35 nm in diameter embedded in the amorphous silica-alumina matrix. The new adsorbent showed excellent adsorption capacity for methylene blue dye. The nanocomposites removal rate strongly depended on the heat-treatment temperature of absorbent and contact time. The maximum dye removal was obtained for the samples calcined at 650 °C.

References

- Ahmad M, Ahmed E, Hong ZL, Khalid NR, Ahmed W, Elhissi A (2013) *J Alloys Compd* 577:717
- Panda N, Sahoo H, Mohapatra S (2011) *J Hazard Mater* 185:359
- Chung KT, Stevens SE (1993) *Toxicol Chem* 12:2121
- Chung KT, Stevens SE, Cerniglia CE (1992) *Crit Rev Microbiol* 18:175
- Crini G (2003) *Bioresour Technol* 90:193
- Shuang CD, Li PH, Li AM, Zhou Q, Zhang MC, Zhou Y (2012) *Water Res* 46:4417
- Yan H, Li H, Yang H, Li A, Cheng R (2013) *Chem Eng J* 223:402
- Deligeer W, Gao YW, Asuha S (2011) *Appl Surf Sci* 257:33524
- Anbia M, Hariri SA, Ashrafzadeh SN (2010) *Appl Surf Sci* 256:3228
- Hou H, Zhou R, Wu P, Wu L (2012) *Chem Eng J* 211:336
- Travlou NA, Kyzas GZ, Lazaridis NK, Deliyanni EA (2013) *Chem Eng J* 217:256
- Tajizadegan H, Jafari M, Rashidzadeh M, Saffar-Teluri A (2013) *Appl Surf Sci* 276:317
- Kun-hong H, Di-fang Z, Jun-sheng L (2012) *Metal Soc* 22:2484
- Kuznetsov DV, Bardakhanov SP, Nomoev AV, Novopashin SA, Lygdenov VZ (2010) *J Eng Mater Technol* 19:138
- Das M, Prakash Singh SH, Pal K, Jena S, Karmakar B (2010) *J Eng Mater Sci* 17:199
- Ferreira Da Silva MG (1998) *J Sol–Gel Sci Technol* 13:987
- Gnanam S, Rajendran V (2011) *J Sol–Gel Sci Technol* 58:62
- Chou LJ, Cai YC, Zhang B, Niu JZ, Ji SF, Li SB (2003) *Appl Catal A* 238:185
- Han B, Zhang F, Feng Z, Liu S, Deng S, Wang Y (2014) *Ceram Int* 40:8093
- Wu R, Qu J, Chen Y (2005) *Water Res* 39:630
- Yuan M, Wang S, Wang X, Zhao L, Hao T (2011) *Appl Surf Sci* 257:7913
- Wang C, Cao M, Wang P, Ao Y, Hou J, Qian J (2014) *Appl Catal A* 473:83
- Hassanzadeh-Tabrizi SA, Taheri-Nassaj E, Sarpoolaky H (2008) *J Alloys Compd* 456:282
- Hassanzadeh-Tabrizi SA, Taheri-Nassaj E (2010) *J Alloys Compd* 494:289
- Shojaie-Bahaabad M, Taheri-Nassaj E (2008) *Mater Lett* 62:3364
- Sedaghat A, Taheri-Nassaj E, Naghizadeh R (2006) *J Non-Cryst Solids* 352:2818
- Lippens BC, Boer DJH (1964) *Acta Crystallogr* 17:1312
- Tan Z, Qiu J, Kong F, Wang Z, Hao F (2012) *Chem Eng J* 195:218
- Li G, Liu S, Chu Z, Gao H, Wu D, Wu J, Yue D, Wang Z (2012) *J Lumin* 132:2961
- Ali AM, Ismail AA, Najmy R, Al-Hajry A (2014) *J Photochem Photobiol A* 275:37
- Tajer-Kajinebaf V, Sarpoolaky H, Mohammadi T (2014) *Ceram Int* 40:1747
- Sing KSW, Everett DH, Haul RAW, Moscou L, Pierotti RA, Rouquerol J, Siemieniewska T (1985) *Pure Appl Chem* 57:603
- Santos GA, Santos CMB, Silva SW, Urquieta-González EA, Sartoratto PPC (2012) *Colloids Surf A* 395:217
- Chenguo H, Zuwei Z, Hong L, Puxian G, Zhong Lin W (2006) *Nanotechnology* 17:5983
- Tjong SC, Chen H (2004) *Mater Sci Eng R* 45:1
- Pandiselvi K, Thambidurai S (2013) *Colloids Surf B* 108:229